

**Citation for published version:**

Khalfallah Tahir, Cheikh Belfedal, Tayeb Allaoui, Mouloud Denai, and M'hamed Doumi, 'A new sliding mode control strategy for variable-speed wind turbine power maximization', *International Transactions on Electrical Energy Systems*, Vol. 28 (4): e2513, April 2018.

**DOI:**

<https://doi.org/10.1002/etep.2513>

**Document Version:**

This is the Accepted Manuscript version.

The version in the University of Hertfordshire Research Archive may differ from the final published version.

**Copyright and Reuse:**

© 2018 John Wiley & Sons Ltd.

This article may be used for non-commercial purposes in accordance with [Wiley Terms and Conditions for Self-Archiving](#)

**Enquiries**

If you believe this document infringes copyright, please contact Research & Scholarly Communications at [rsc@herts.ac.uk](mailto:rsc@herts.ac.uk)

# A New Sliding Mode Control Strategy for Variable-Speed Wind Turbine Power Maximization

K. Tahir,<sup>1</sup> C. Belfedal,<sup>1</sup> T. Allaoui,<sup>1</sup> M. Denai,<sup>2\*</sup> and M. Doumi<sup>3</sup>

<sup>1)</sup>Department of Electrical Engineering, Ibn Khaldoun University, Tiaret, 14000, Algeria

<sup>2)</sup>School of Engineering Technology, University of Hertfordshire, Hatfield AL10 9AB, UK

<sup>3)</sup>Department of Electrical Engineering, Tahri Mohammed University, Bechar, 8000, Algeria

\*Corresponding author: [m.denai@herts.ac.uk](mailto:m.denai@herts.ac.uk)

## Abstract

The paper proposes a new sliding mode power control strategy for a wound-field synchronous generator (WFSG)-based variable speed wind energy conversion systems (WECS) to maximize the power extracted from the wind turbine. The proposed controller can handle the inherent nonlinearities in WECS and the randomness of the wind speed as well as the uncertainties of the model and external disturbances. To reduce the chattering phenomenon which characterize conventional sliding mode control (SMC), a sigmoid function with a variable boundary layer is proposed. The adaptive switching gains are adjusted on-line using a fuzzy logic-based technique. Several simulation scenarios were performed to evaluate the performance of the proposed control scheme. The results demonstrate that this controller provides excellent response characteristics, is robust against parameter variations and free from chattering phenomenon as compared to the conventional SMC.

**Keywords:** wound field synchronous generator, wind energy conversion systems, Maximum Power Point tracking, sliding mode control, fuzzy logic, chattering phenomenon

## I. INTRODUCTION

Like solar, wind energy has an enormous potential to address the rapidly increasing demand for energy, alleviate the problem of global warming and contribute to sustainable development [1].

Wind technology has experienced a very fast development over the last decade and, currently, variable-speed wind turbines have become the industry standard due of their ability to achieve maximum efficiency under various wind speeds conditions and to deliver better power quality over their fixed speed counterparts. Furthermore, a maximum power point control strategy is essential to determine the turbine speed to capture the maximum power from the wind [2].

Several types of electric generators have been used in WECSs including Squired-Cage Induction Generator (SCIG), Synchronous Generator with external field excitation, Doubly Fed Induction Generator (DFIG) and Permanent Magnet Synchronous Generator (PMSG) [3].

The primary advantage of Wound Field Synchronous Generators (WFSG) is its high efficiency because the whole stator current is used to produce the electromagnetic torque [4]. The main benefit of the WFSG with salient pole is that it allows a direct control of the power factor of the machine, consequently the stator current may be reduced under these circumstances [5].

A WECS exhibits variability in the output power due to the intermittent nature of wind speed which depends on the environmental conditions. These inherent nonlinear characteristics and uncertainties in the system dynamics makes the control of WECS a rather challenging task.

Various methods have been proposed for controlling the WECS: The authors in [6, 7] proposed fuzzy logic control to enhance the performance of the WECS in terms of reference tracking and sensitivity to parameter variations. In [8], a comparative study between the polynomial RST control and linear quadratic Gaussian (LQG) control under wind turbine system parameters variations is presented. A hybrid control that improves the dynamic performance of wind turbines based on a wound field synchronous generator is presented in [9]. Also, a hybrid fuzzy sliding mode controller is proposed in [10]. In [11], the authors used model reference adaptive control and neuro-fuzzy control to overcome the drawbacks of classical PID controllers.

One of the most important problems in developing WECS is associated with the design of robust control strategies with low computational time and capable of optimizing the efficiency of the system while decreasing structural loading. Variable structure control theory with sliding mode has evolved for many years as a robust control methodology for nonlinear systems with parameter uncertainties. Among the several features of SMC, the most attractive are good performance against un-modeled dynamics, insensitivity to parameter variation, external disturbance rejection and fast dynamic response [12].

A major drawback of the classical SMC is the chattering phenomenon caused by the switching gain and the discontinuous form of the switching function. This problem has been studied extensively by many authors and several methods have been proposed in the literature.

In [13], the authors used a saturation function in the SMC with an equivalent control feedback technique. However, the introduction of a low-pass filter usually causes a phase delay and hence high-performance control requirements cannot be met. To overcome the time delay caused by the low-pass filter, the authors in [14], introduced a sigmoidal switching function with a variable boundary layer instead of the conventional sign function and in [15], a hyperbolic tangent function is used to alleviate the discontinuous function and was applied to a DFIG wind turbine

system. Various complex hybrid structures have also been proposed to enhance the asymptotic stability and reduce the chattering phenomenon by combining SMC with adaptive control and fuzzy control techniques [16, 17]. A novel adaptive terminal sliding mode instantaneous active and reactive power control is proposed in [18]. However, most of these hybrid controllers are difficult to design and implement.

However, all these methods do not consider the value of the switching gain even though this latter is directly proportional to the chattering level.

In brief, the motivation for this research paper is to study the WECS response during dynamic changes in wind speed and also against parameter variations, and to propose a new control strategy based on sliding mode control to: (1) mitigate the problems associated with the conventional SMC such as the chattering phenomenon, (2) improve wind energy conversion efficiency, and (3) enhance the performance of the system.

A state-dependent gain scheduling method for adjusting the thickness of boundary layer based on a fast sigmoid function is designed while the switching gain is adjusted using a fuzzy logic control (FLC) technique to mitigate the effect of chattering in SMC.

In order to show the superiority of the proposed SMC technique, its performances were compared to those of the conventional SMC, FLC controller and a PI controller under different operating conditions.

This paper is organized as follows: Section II presents a description of the WFSG-based WECS and the modeling of the systems' components (wind turbine and gearbox, WFSG). Field oriented control (FOC) of the WFSG is developed in Section III. The proposed SMC technique is discussed in Section V and its application for the WECS is derived in Section VI. Section IX presents the simulation results and discussions and finally, the conclusions of the work are summarized in Section X.

## II. WIND CONVERSION SYSTEM MODEL

Fig. 1 depicts the WECS used in this study. The wind turbine shaft is connected to the WFSG rotor through a gearbox which adapts the slow speed of the turbine to the WFSG speed. The rotor winding of the WFSG is connected to the DC bus via a DC/DC converter, whereas the stator winding is fed by a back-to-back bidirectional Pulse Width Modulation Voltage Source Converter (PWM-VSC), which is connected to the grid via an RL filter. The back-to-back converter consists of two converters; a Machine Side Converter (MSC) and a Grid Side Converter (GSC), which are connected through a common DC-link.

The control system of the WECS consists of the generator side and grid side controllers. The GSC regulates the DC-link voltage and also controls the reactive power exchange between the generator and the grid. The role of the MSC is to maintain a decoupling between the stator side active and reactive powers by adjusting the direct and quadrature components of the WFSG stator current. The Maximum Power Point Tracking (MPPT) algorithm of the turbine is based on the tip speed ratio (TSR) method.

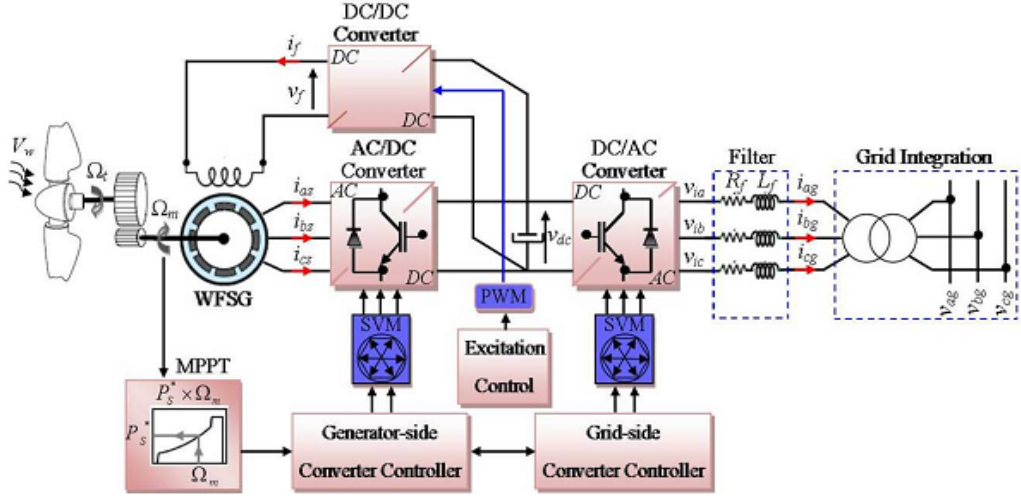


Fig. 1 Wind energy conversion system structure.

#### A. Modeling of the wind turbine and gearbox

The aerodynamic power developed by the wind turbine is given by the following equation [19, 20]:

$$P_a = \frac{1}{2} \rho \pi R^2 V_w^3 C_p(\lambda, \beta) \quad (1)$$

Where  $\rho$  is the air density,  $R$  is the wind turbine blade radius,  $V_w$  is the wind velocity (m/s) and  $C_p$  is called the power coefficient, which is a function of both the blade pitch angle  $\beta$  and the TSR  $\lambda$  which is defined as [21]:

$$\lambda = \frac{R\Omega_t}{V_w} \quad (2)$$

Where  $\Omega_t$  is the speed of the wind turbine. The  $C_p(\lambda, \beta)$  characteristic is illustrated in Fig. 2.

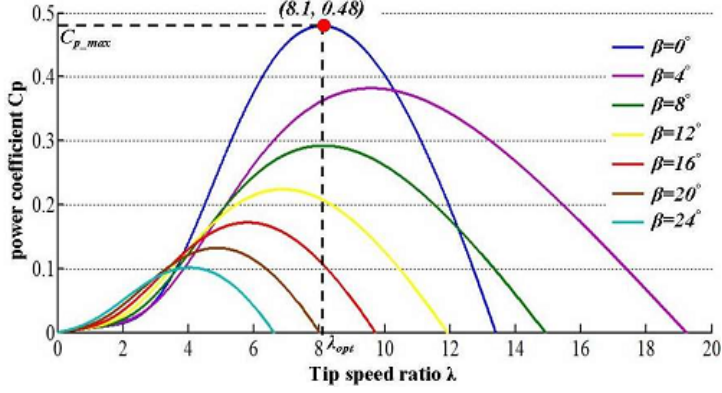


Fig. 2 Power coefficient versus tip speed ratio.

It can be noticed that for a given  $\beta$ , there is one value of  $\lambda(\lambda_{opt})$  for which  $C_p$  is maximum. In addition, when  $\beta = 0$ , the turbine has a maximum efficiency: ( $C_{p,max} = 0.48$ ,  $\lambda_{opt} = 8.1$ ).

The mechanical equation of the generator is given by:

$$J \frac{d\Omega_m}{dt} = T_m - T_{em} - f\Omega_m \quad (3)$$

Where  $J$  and  $f$  are the total inertia and the viscous friction coefficient appearing at the generator side,  $T_m$  is the gearbox torque,  $T_{em}$  is the generator torque, and  $\Omega_m$  is the generator's mechanical speed.

$$T_m = \frac{T_a}{G} \quad \Omega_t = \frac{\Omega_m}{G} \quad T_a = \frac{P_a}{\Omega_t} \quad (4)$$

Where  $G$  is the gear ratio, and  $T_a$  denotes the aerodynamic torque.

The TSR method determines the optimal speed of the turbine to harvest the maximum power from the wind. From (2), the optimal turbine speed is achieved when tip speed- ratio is optimal. Therefore, the speed of the wind turbine should be maintained at the following reference:

$$\Omega_{t\_ref} = \frac{\lambda_{opt} V_w}{R} \quad (5)$$

## B. Modeling of the WFSG

The generator voltage equations in the rotating  $d-q$  reference frame are obtained as follows [22]:

$$\begin{cases} v_{ds} = -r_s i_{ds} + \omega_e L_q i_{qs} - \omega_e M_{SQ} i_Q - L_d \frac{di_{ds}}{dt} + M_{sf} \frac{di_f}{dt} + M_{SD} \frac{di_D}{dt} \\ v_{qs} = -r_s i_{qs} - \omega_e L_d i_{ds} + \omega_e M_{sf} i_f + \omega_e M_{SD} i_D - L_q \frac{di_{qs}}{dt} + M_{SQ} \frac{di_Q}{dt} \\ v_f = r_f i_f + L_f \frac{di_f}{dt} - M_{sf} \frac{di_{ds}}{dt} + M_{fD} \frac{di_D}{dt} \\ 0 = r_D i_D + M_{fD} \frac{di_f}{dt} - M_{SD} \frac{di_{ds}}{dt} + L_D \frac{di_D}{dt} \\ 0 = r_Q i_Q - M_{SQ} \frac{di_{qs}}{dt} + L_Q \frac{di_Q}{dt} \end{cases} \quad (6)$$

The electrical angular speed of the WFSG is:

$$\omega_e = p\Omega_m \quad (7)$$

The electromagnetic torque is expressed by:

$$T_{em} = p(\phi_{ds} i_{qs} - \phi_{qs} i_{ds}) = p[(L_q - L_d) i_{ds} i_{qs} + (M_{sf} i_f + M_{SD} i_D) i_{qs} - M_{SQ} i_Q i_{ds}] \quad (8)$$

### III. FIELD ORIENTED CONTROL OF A WFSG

The principle of vector control of WFSG is based on the orientation of the rotor flux along the *d*-axis. This strategy consists of keeping the *d*-axis constantly aligned with the magnetic axis of the rotor field. This orientation leads to setting the *d*-axis stator current  $i_{ds} = 0$ , a simple control of the power can be achieved through the control of the quadrature current only [23].

Under this condition, the electromagnetic torque becomes:

$$T_{em} = p i_{qs} (M_{sf} i_f + M_{SD} i_D) \quad (9)$$

The reference signals  $i_{qs\_ref}$  and  $i_{f\_ref}$  are derived from (9) as follows:

$$i_{qs\_ref} = \frac{T_{em\_ref}}{p(M_{sf} i_f + M_{SD} i_D)} \quad (10)$$

$$i_{f\_ref} = \frac{T_{em\_ref}}{p M_{sf} i_{qs\_ref}} - \frac{M_{SD} i_D}{M_{sf}} \quad (11)$$

The dampers action occurs whenever the rotary field is varied (fast load change, pulsation in the torque of the machine). Induced currents arise in the absorber and produce a torque that dampens oscillations and maintains the synchronism.

During steady-state (constant speed, constant torque), the two current  $i_D$  and  $i_Q$  are zero since there is no relative movement between the rotating field winding and dampers. Therefore, the decoupled control strategy of *d* and *q* current loops (the first two equations of (6)) can be re-written as follows:

$$\begin{cases} v_{ds} = - \left( r_s i_{ds} - L_d \frac{di_{ds}}{dt} \right) + \omega_e L_q i_{qs} - \omega_e M_{sQ} i_Q \\ v_{qs} = - \left( r_s i_{qs} - L_q \frac{di_{qs}}{dt} \right) - \omega_e L_q i_{ds} + \omega_e M_{sf} i_f + \omega_e M_{sD} i_D \end{cases} \quad (12)$$

Where the terms in brackets in equation (12) are used to design the inner control loop in the  $d$ - $q$  axis, while the others terms are considered as compensating or disturbance terms [24].

#### IV. DESIGN OF THE SMC

Let the nonlinear dynamical system be defined as [25, 26]:

$$\begin{cases} x^{(n)}(t) = f(x(t), t) + g(x(t), t)u(t) + d(t) \\ y(t) = x(t) \end{cases} \quad (13)$$

Where  $x = [x(t) \quad \dot{x}(t) \quad \dots \quad x^{(n)}(t)]^T$  denotes the state vector,  $f(x(t), t)$  and  $g(x(t), t)$  are nonlinear function,  $u(t)$  is the control input,  $d(t)$  is the external disturbances.

The aim is to find a control input signal  $u(t)$  which forces the output  $y(t)$  in (13) to follow a given bounded reference signal  $y_d(t)$ , that is, the tracking error  $e(t) = y_d(t) - y(t)$  and its forward shifted values, defined as:

$$\left\{ \begin{array}{l} e^{(i)}(t) = y_d^{(i)}(t) - y^{(i)}(t) \\ (i = 1, \dots, \dots, n-1) \end{array} \right. \quad (14)$$

The design of the SMC is performed in two steps: i) Selection of the switching hyper-plane to impose the desired dynamics for the controlled system, ii) Design of the discontinuous control such that the system enters the sliding mode regime and remains there [25, 27]. In the proposed SMC control scheme, the following sliding surface is used [25]:

$$s(x, t) = \left( \frac{d}{dt} + \lambda \right)^{n-1} e(t) \quad (15)$$

Where  $e(t) = x_d(t) - x(t)$ ,  $\lambda$  is a positive coefficient and  $n$  denotes the order of the system.

Consider the following Lyapunov function:

$$V = \frac{1}{2} s^2 \quad (16)$$

Lyapunov theorem states that if  $\dot{V}$  is negative definite, then the system trajectory will converge towards the sliding surface and will remain there until the origin is reached asymptotically:

$$\dot{V} = s\dot{s} \quad (17)$$

A sufficient condition for stability is:

$$\frac{1}{2} \frac{d}{dt} s^2 = s\dot{s} \leq -\eta |s| \quad (18)$$

Where  $\eta$  is a strictly positive constant.

The sliding control law  $u(t)$  is defined as:

$$\begin{cases} u(t) = u_{eq}(t) + u_n(t) \\ u_n(t) = -K \cdot \text{signum}(s(x, t)) \end{cases} \quad (19)$$

Where  $u_{eq}(t)$  and  $u_n(t)$  denote the equivalent and the switching controls respectively,  $K$  represents the controller gain and  $\text{signum}(s(x, t))$  is a signum function defined as:

$$\text{signum}(s(x, t)) = \begin{cases} -1 & \text{if } s(x, t) < 0 \\ 1 & \text{if } s(x, t) > 0 \end{cases} \quad (20)$$

## V. PROPOSED SLIDING MODE CONTROL

The conventional SMC uses the signum function as a switching function and hence suffers from chattering. In the proposed SMC scheme, this discontinuous function is replaced with the following fast-continuous sigmoid function [28]:

$$\text{sigmoid}(\rho, s) = \frac{\lambda s}{\rho + |\lambda s|} \quad (21)$$

Where  $\rho$  is a state-dependent small positive constant of the thickness of the boundary layer and  $\lambda$  is positive constant used to adjust the tuning rate of the sigmoid function. The boundary layer is obtained from the proposed state-dependent variable of the sigmoid function as:

$$\rho = (1 - |\text{sigmoid}(\rho, s)|) - \delta_1 \quad (22)$$

Where  $\delta_1$  is a sufficiently small constant. When the uncertainties are large,  $\rho$  will produce a small boundary layer to improve the control accuracy and achieve a better tracking performance.

Fig. 3 illustrates how the boundary layer is adjusted according to the parameters  $\lambda$  and  $\rho$  which determine the steepness of the function  $\text{sigmoid}(\rho, s)$ .

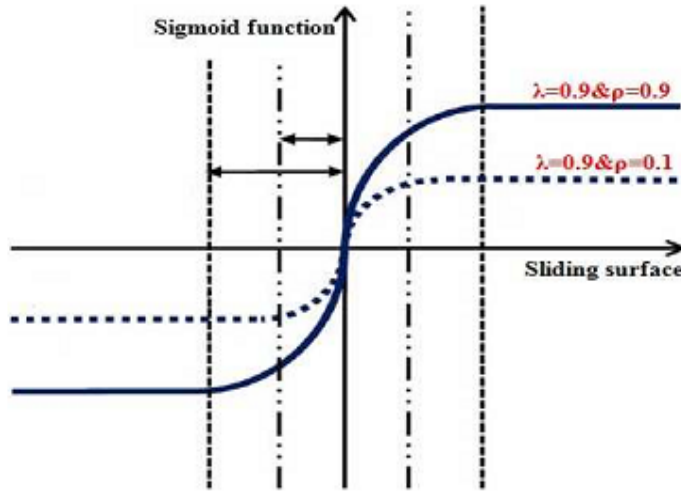


Fig. 3 Variable boundary layers for different values of  $\lambda$  and  $\rho$ .

Large values of the switching gain  $K$  produce larger and faster switching action during the crossing of the sliding surface which will, in turn, result in unwanted chattering in the system. To overcome this, a set of fuzzy logic rules are used to adjust the switching gains with the state of the sliding surface.

## VI. APPLICATION OF THE PROPOSED SMC TO THE WFSG

### A. Speed control surface

The first order tracking error dynamics of the proposed sliding surface is equal to the error between the actual and the reference speed:

$$s(\Omega_m) = e(\Omega_m) = \Omega_{m\_ref} - \Omega_m \quad (23)$$

Taking the derivative of (23) gives:

$$\dot{s}(\Omega_m) = \dot{\Omega}_{m\_ref} - \dot{\Omega}_m \quad (24)$$

Substituting (3) into (24) leads to:

$$\dot{s}(\Omega_m) = \gamma_2 \Omega_m - \gamma_1 + \dot{\Omega}_{m\_ref} + \gamma_3 (M_{sf} i_f + M_{sd} i_D) i_{qn} \quad (25)$$

$$\gamma_1 = T_a/J \quad \gamma_2 = f/J \quad \gamma_3 = p/J$$

Now, replacing the current  $i_q$  with the control current  $i_{q\_ref} = i_{qe\_eq} + i_{qn}$  in (25), gives:

$$\begin{aligned} \dot{s}(\Omega_m) = & \gamma_2 \Omega_m - \gamma_1 + \dot{\Omega}_{m\_ref} + \gamma_3 (M_{sf} i_f + M_{sd} i_D) i_{qe\_eq} \\ & + \gamma_3 (M_{sf} i_f + M_{sd} i_D) i_{qn} \end{aligned} \quad (26)$$

During the sliding mode and the steady state, we have  $s(\Omega_m) = 0$  and consequently  $\dot{s}(\Omega_m) = 0$  and  $i_{qn} = 0$ . Hence, solving for the equivalent control gives:

$$i_{qe\_eq} = \frac{-\gamma_2 \Omega_m + \gamma_1 - \dot{\Omega}_{m\_ref}}{\gamma_3 (M_{sf} i_f + M_{sd} i_D)} \quad (27)$$

After convergence, the condition  $s(\Omega_m)\dot{s}(\Omega_m) < 0$  must be verified. Substituting (27) in (26) yields:

$$\dot{s}(\Omega_m) = \gamma_3 (M_{sf} i_f + M_{sd} i_D) i_{qn} \quad (28)$$

The following soft control law is applied:

$$i_{qn} = K_{\Omega_m} \cdot \text{sigmoid}(\rho, s(\Omega_m)) \quad (29)$$

### B. Surfaces for the control of stator currents

The following surfaces are used:

$$\begin{cases} S(i_{ds}) = i_{ds\_ref} - i_{ds} \\ S(i_{qs}) = i_{qs\_ref} - i_{qs} \end{cases} \quad (30)$$

Taking the derivatives gives:

$$\begin{cases} \dot{S}(i_{ds}) = \frac{di_{ds\_ref}}{dt} - \frac{di_{ds}}{dt} \\ \dot{S}(i_{qs}) = \frac{di_{qs\_ref}}{dt} - \frac{di_{qs}}{dt} \end{cases} \quad (31)$$

Substituting the expressions of the derivatives of the stator currents given by equations (12) into (31) yields:

$$\begin{cases} \dot{S}(i_{ds}) = \frac{di_{ds\_ref}}{dt} + \frac{r_s}{L_d} i_{ds} + \frac{b_1}{L_d} i_{qs} - \frac{b_2}{L_d} i_Q - \frac{M_{sf}}{L_d} \frac{di_f}{dt} - \frac{M_{SD}}{L_d} \frac{di_D}{dt} + \frac{v_d}{L_d} \\ \dot{S}(i_{qs}) = \frac{di_{qs\_ref}}{dt} + \frac{r_s}{L_q} i_{qs} + \frac{b_1}{L_q} i_{ds} - \frac{b_2}{L_q} i_Q - \frac{M_{sf}}{L_q} \frac{di_f}{dt} - \frac{M_{SD}}{L_q} \frac{di_D}{dt} + \frac{v_q}{L_q} \end{cases} \quad (32)$$

Replacing the voltages  $v_d$  and  $v_q$  with  $v_{d\_ref} = v_{deq} + v_{dn}$  and  $v_{q\_ref} = v_{qe eq} + v_{qn}$  respectively, gives:

$$\begin{cases} \dot{S}(i_{ds}) = \frac{di_{ds\_ref}}{dt} + \frac{r_s}{L_d} i_{ds} + \frac{b_1}{L_d} i_{qs} - \frac{b_2}{L_d} i_Q - \frac{M_{sf}}{L_d} \frac{di_f}{dt} - \frac{M_{SD}}{L_d} \frac{di_D}{dt} + \frac{1}{L_d} (v_{deq} + v_{dn}) \\ \dot{S}(i_{qs}) = \frac{di_{qs\_ref}}{dt} + \frac{r_s}{L_q} i_{qs} + \frac{b_1}{L_q} i_{ds} - \frac{b_2}{L_q} i_Q - \frac{M_{sf}}{L_q} \frac{di_f}{dt} - \frac{M_{SD}}{L_q} \frac{di_D}{dt} + \frac{1}{L_q} (v_{qe eq} + v_{qn}) \end{cases} \quad (33)$$

During slip mode and under steady-state,  $S(i_{ds})\dot{S}(i_{ds}) < 0$  and  $S(i_{qs})\dot{S}(i_{qs}) < 0$ . Consequently,  $v_{dn} = 0$ ,  $\dot{S}(i_{qs}) = 0$  and  $v_{qn} = 0$ . From equations (33) the equivalent controls voltages  $v_{deq}$  and  $v_{qe eq}$  are obtained as:

$$\begin{cases} v_{deq} = -L_d \frac{di_{ds\_ref}}{dt} - r_s i_{ds} + b_1 i_{qs} - b_2 i_Q + M_{sf} \frac{di_f}{dt} + M_{SD} \frac{di_D}{dt} \\ v_{qe eq} = -L_q \frac{di_{qs\_ref}}{dt} - r_s i_{qs} - a_1 i_{ds} + a_2 i_f + a_3 i_D + M_{SQ} \frac{di_Q}{dt} \end{cases} \quad (34)$$

During the convergence mode, the conditions  $S(i_{ds})\dot{S}(i_{ds}) < 0$  and  $S(i_{qs})\dot{S}(i_{qs}) < 0$  must be satisfied. Substituting equations (34) into (33) respectively, gives:

$$\begin{cases} \dot{S}(i_{ds}) = \frac{1}{L_d} v_{dn} \\ \dot{S}(i_{qs}) = \frac{1}{L_q} v_{qn} \end{cases} \quad (35)$$

With

$$\begin{cases} v_{dn} = K_{i_{ds}} \cdot \text{sigmoid}(\rho, s(i_{ds})) \\ v_{qn} = K_{i_{qs}} \cdot \text{sigmoid}(\rho, s(i_{qs})) \end{cases} \quad (36)$$

The positive coefficients in equations (27) and (34) are given by:

$$\begin{array}{lll} a_1 = L_d \omega_e & a_2 = M_{sf} \omega_e & a_3 = M_{sd} \omega_e \\ b_1 = L_q \omega_e & b_2 = M_{sq} \omega_e \end{array}$$

## VII. SWITCHING GAINS ADAPTATION USING FUZZY RULES

When the system state trajectory is far from the sliding surface, which means the value of  $|S|$  is large, the switching gains  $K_{\Omega_m}$ ,  $K_{ids}$  and  $K_{iqs}$  should be increased to drive the trajectory back. On the other hand, when the value of  $|S|$  is small, the gains should be reduced. Hence fuzzy logic rules can be used to adjust the switching gains according to the value of  $|S|$ .

The fuzzy rules for the speed and current controllers are shown in Tables 1 and 2 respectively.

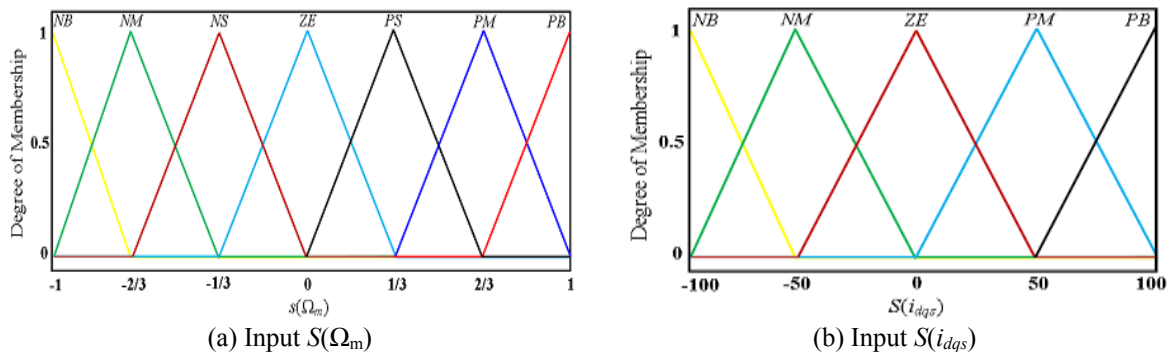
Table 1 Fuzzy rules for the speed controller.

$S(\Omega_m)$	PB	PM	PS	ZE	NS	NM	NB
$u(\Omega_m)$	PB	PM	PS	ZE	PS	PM	PB

Table 2 Fuzzy rules for the current controller.

$S(i_{dqs})$	NB	NM	ZE	PM	PB
$u(i_{dqs})$	Bigger	Big	Medium	Small	Smaller

The fuzzy sets are labeled as NB (Negative Big), NM (Negative Medium), NS (Negative Small) and ZE (Zero), PB (Positive Big), PM (Positive Medium), PS (Positive Small). The membership functions of the inputs  $S(\Omega_m)$ ,  $S(i_{dqs})$  and outputs  $u(\Omega_m)$ ,  $u(i_{dqs})$  are shown in Fig. 4.



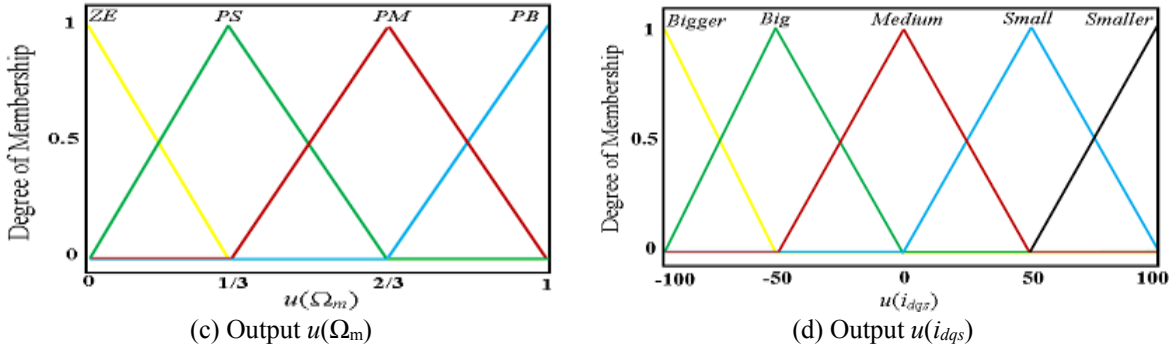


Fig. 4 Membership functions of the input and output of the FLC.

In the fuzzy logic rules scheme, output  $u$  is computed by a mechanism of If–Then rules. Here, the general type of If–Then rules will be used in the following form:

*Rule (i): If  $x_i$  is  $F(x_i)$ , then  $y_i$  is  $F(y_i)$*

Where  $x_i$  are input linguistic variables and  $y_i$  are output linguistic variables;  $F(x_i)$  and  $F(y_i)$  are membership functions. For example the fuzzy rules of speed controllers are defined as follows.

*Rule 1: If  $S$  is PB, then  $u$  is PB.*

If ( $S = \text{PB}$ ) so ( $|S| = \text{PB}$ ) then the measured speed is much lower than the reference speed. To make it return to the reference speed it must be increased rapidly, i.e. apply a large increase in the control variable  $u$ . That is to say ( $u = \text{PB}$ ). The same procedure for the following rules.

*Rule 2: If  $S$  is PM, then  $u$  is PM.*

*Rule 3: If  $S$  is PS, then  $u$  is PS.*

*Rule 4: If  $S$  is ZE, then  $u$  is ZE.*

*Rule 5: If  $S$  is NS, then  $u$  is PS.*

*Rule 6: If  $S$  is NM, then  $u$  is PM.*

*Rule 7: If  $S$  is NB, then  $u$  is PB.*

Finally, the fuzzy outputs are defuzzified using the center of area method and multiplied by the scaling gains  $K_{\Omega_m}$ ,  $K_{ids}$  and  $K_{iqs}$  to generate the control signals. Therefore, the new gains of the controller will be:  $K'_{\Omega_{mec}} = u(\Omega_m) \cdot K_{\Omega_m}$ ;  $K'_{ids} = u(i_{ds}) \cdot K_{ids}$  and  $K'_{iqs} = u(i_{qs}) \cdot K_{iqs}$ .

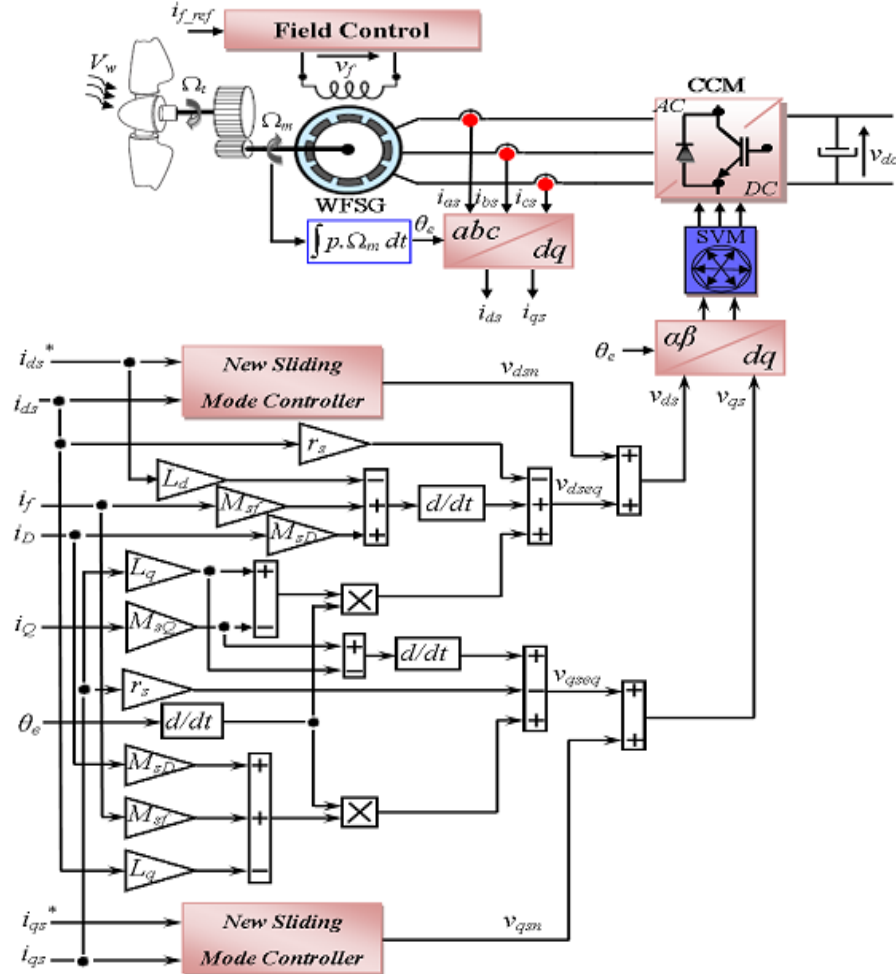


Fig. 5 Block diagram of the MSC control based on the proposed SMC.

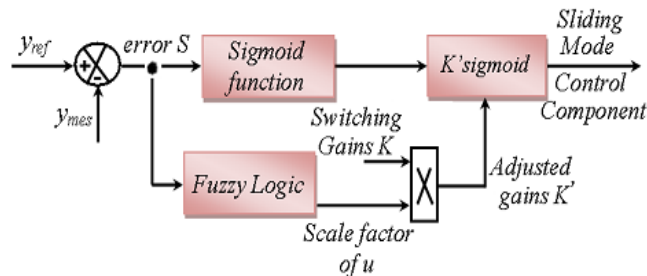


Fig. 6 Structure of the SMC.

Fig. 5 depicts the proposed MSC control scheme. The "new sliding mode controller" bloc is detailed in Fig. 6.

## VIII. CONTROL OF GRID-SIDE CONVERTER

The control of the grid-side converter is based on the assumption that the  $d$ -axis is oriented along the grid voltage vector position, that is,  $v_{qg} = 0$  and thus the grid voltage has a  $d$ -axis

component  $v_{dg}$  only [29]. Therefore, the dynamic model of the GSC in the reference frame rotating synchronously can be expressed as [30, 31]:

$$\begin{cases} v_{df} = R_f i_{df} + L_f \frac{di_{df}}{dt} - \omega L_f i_{qf} + v_g \\ v_{qf} = R_f i_{qf} + L_f \frac{di_{qf}}{dt} + \omega L_f i_{df} \end{cases} \quad (37)$$

Where  $v_{df}$ ,  $v_{qf}$  are the inverter  $d$ -axis and  $q$ -axis voltage components;  $v_g$  is the grid voltage component along the  $d$ -axis;  $i_{df}$ ,  $i_{qf}$  is the  $d$  and  $q$ -axis currents of the grid;  $R_f$  and  $L_f$  represents the filter resistance and inductance respectively and  $\omega$  is the network angular frequency.

Then, the active and reactive powers injected by the GSC into the grid are given by:

$$\begin{cases} P_g = \frac{3}{2} (v_{dg} i_{df} + v_{qg} i_{qf}) = \frac{3}{2} v_g i_{df} \\ Q_g = \frac{3}{2} (v_{qg} i_{df} - v_{dg} i_{qf}) = -\frac{3}{2} v_g i_{qf} \end{cases} \quad (38)$$

It can be observed from equation (48), that the real and reactive power control can be achieved by controlling direct and quadrature current components, respectively.

Therefore, the reference values of  $i_{df}$  and  $i_{qf}$  are:

$$\begin{cases} i_{df\_ref} = \frac{2 P_{g\_ref}}{3 v_g} \\ i_{qf\_ref} = -\frac{2 Q_{g\_ref}}{3 v_g} \end{cases} \quad (39)$$

There are also two control loops for the network side power converter system. An inner loop to control the line current and an outer loop to regulate the DC bus voltage.

#### A. Control scheme of the outer-loop

For the DC-link voltage controller, the sliding surface is set as:

$$S(v_{dc}) = v_{dc\_ref} - v_{dc} \quad (40)$$

When the sliding surface is reached and the system state is in equilibrium, then:

$$\dot{S}(v_{dc}) = \frac{dS(v_{dc})}{dt} = -\frac{dv_{dc}}{dt} = 0 \quad (41)$$

The reference for the real power injected into the grid is given by:

$$P_{g\_ref} = \left( i_{ms} - C \frac{dv_{dc}}{dt} \right) v_{dc} \quad (42)$$

Where  $v_{dc}$  is the DC-link voltage;  $i_{ms}$  is the machine side transmission line current; and  $C$  is the DC-link capacitor.

The controller is designed to generate the reference for the real power which is the input to the inner loop. Thus (42) is rewritten as:

$$P_{g\_ref} = \left( i_{ms} + C \frac{dS(v_{dc})}{dt} \right) v_{dc} \quad (43)$$

To ensure the attractiveness condition  $S(x)\dot{S}(x) < 0$  and  $\dot{S}(x)$  is chosen as follow:

$$\frac{dS(v_{dc})}{dt} = -K_1 S(v_{dc}) - K_2 \cdot \text{sigmoid}(\rho, S(v_{dc})) \quad (44)$$

Where  $K_1$  and  $K_2$  are positive control gains.

## B. Control scheme of the inner-loop

The switching surfaces for  $i_{df}$  and  $i_{qf}$  are defined as:

$$\begin{cases} S(i_{df}) = i_{df\_ref} - i_{df} \\ S(i_{qf}) = i_{qf\_ref} - i_{qf} \end{cases} \quad (45)$$

It follows that:

$$\begin{cases} \dot{S}(i_{df}) = \frac{di_{df\_ref}}{dt} - \frac{di_{df}}{dt} \\ \dot{S}(i_{qf}) = \frac{di_{qf\_ref}}{dt} - \frac{di_{qf}}{dt} \end{cases} \quad (46)$$

From (37), the derivatives of the direct and quadrature currents of the grid can be computed as:

$$\begin{cases} \frac{di_{df}}{dt} = \frac{1}{L_f} (v_{df} - R_f i_{df} + \omega L_f i_{qf} - v_g) \\ \frac{di_{qf}}{dt} = \frac{1}{L_f} (v_{qf} - R_f i_{qf} - \omega L_f i_{df}) \end{cases} \quad (47)$$

Substituting equations (39), (47) into (46), gives:

$$\begin{cases} \dot{S}(i_{df}) = \frac{2}{3} \frac{\dot{P}_{g\_ref}}{v_g} - \frac{1}{L_f} (v_{df} - R_f i_{df} + \omega L_f i_{qf} - v_g) \\ \dot{S}(i_{qf}) = -\frac{2}{3} \frac{\dot{Q}_{g\_ref}}{v_g} - \frac{1}{L_f} (v_{qf} - R_f i_{qf} - \omega L_f i_{df}) \end{cases} \quad (48)$$

When the sliding mode is reached, then:

$$\begin{cases} S(i_{df}) = \dot{S}(i_{df}) = 0 \\ S(i_{qf}) = \dot{S}(i_{qf}) = 0 \end{cases} \quad (49)$$

Combining (48) and (49), the  $d$ - and  $q$ -axis components of the control voltage are obtained as:

$$\begin{cases} v_{deq} = \frac{2}{3} \frac{\dot{P}_{g\_ref} L_f}{v_g} + R_f i_{df} - \omega L_f i_{qf} + v_g \\ v_{qe eq} = -\frac{2}{3} \frac{\dot{Q}_{g\_ref} L_f}{v_g} + R_f i_{qf} + \omega L_f i_{df} \end{cases} \quad (50)$$

$$\begin{cases} v_{dn} = K_{i_{df}} \cdot \text{sigmoid}(\rho, s(i_{df})) \\ v_{qn} = K_{i_{qf}} \cdot \text{sigmoid}(\rho, s(i_{qf})) \end{cases} \quad (51)$$

Following the same strategy presented in Section 7, the new gains of the controller were defined as  $K'_{i_{df}} = u(i_{df}) \cdot K_{i_{df}}$  and  $K'_{i_{qf}} = u(i_{qf}) \cdot K_{i_{qf}}$ . The membership functions of the inputs  $S(i_{dqf})$  and outputs  $u(i_{dqf})$  are shown in Fig. 7 and Fig. 8 respectively.

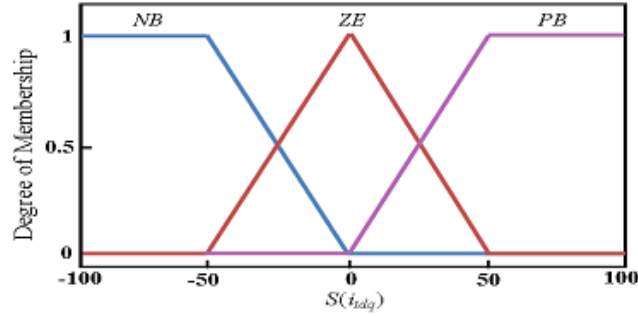


Fig. 7 Membership function for input  $S(i_{dqf})$ .

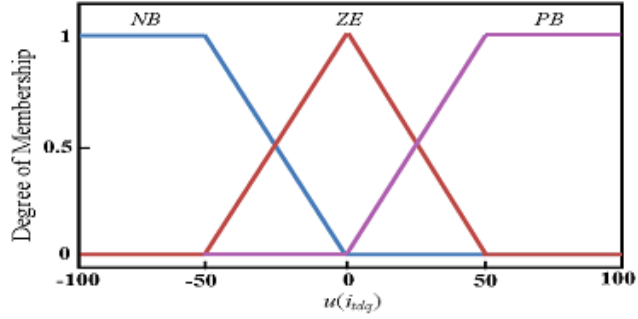


Fig. 8 Membership function for output  $u(i_{dqf})$ .

Finally, the SVPWM (Space Vector Pulse Width Modulation) technique is used to generate gate signals for the converter switches. The control block diagram of the GSC is shown in Fig. 9.

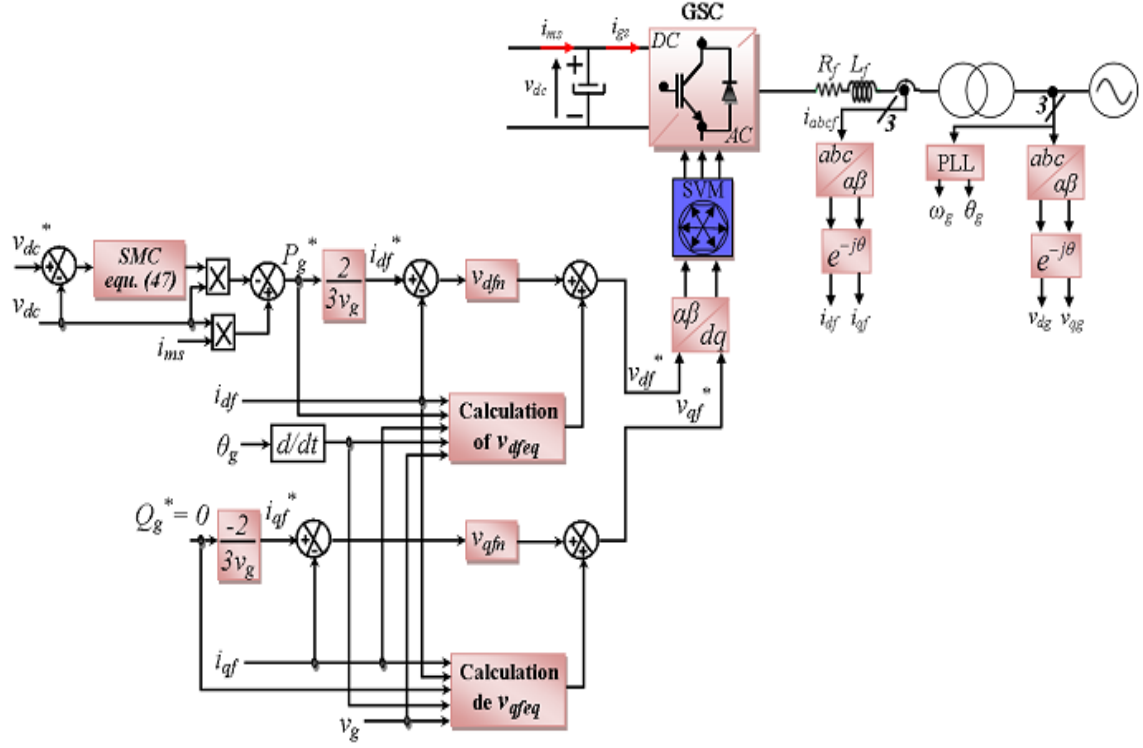


Fig. 9 Block diagram of the GSC control by the proposed SMC.

## IX. SIMULATION RESULTS

The WECS model and the proposed control schemes are implemented using Matlab/Simulink. The model parameter values used in the simulations are listed in Appendix B. In the following simulations, the proposed SMC control scheme is compared with the conventional SMC and other controllers (FLC and PI). Two wind profile scenarios are considered below.

### A. Step change-like wind profile

In this case, the simulation results at the machine-side are presented. The wind speed used has the form of a step variations as shown in Fig. 10. Figs. (11) - (15) show the results obtained for the two controllers: the conventional SMC using a sign function and the proposed SMC based sigmoid function and fuzzy logic.

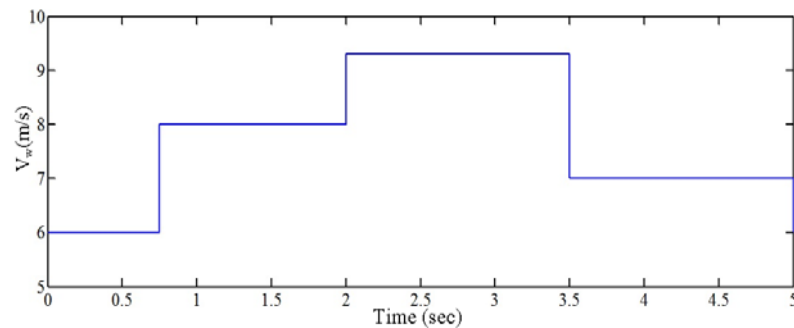


Fig. 10 Wind speed profile.

Both controllers achieved good performance during the transient and steady state regimes. The mechanical rotation speed follows perfectly the speed reference with no overshoot/undershoots and with a minimum response time following a step change in the wind speed as shown in Figs. 12(a) and 12(c).

As shown in Figs. 11(a) and 11(b), the maximum power coefficient value was almost achieved for both controllers. From Figs. 13(a) and 13(b), it can be seen that, with the proposed controller, the electromagnetic torque follows perfectly the optimum torque imposed by the MPPT algorithm as compared to the conventional SMC.

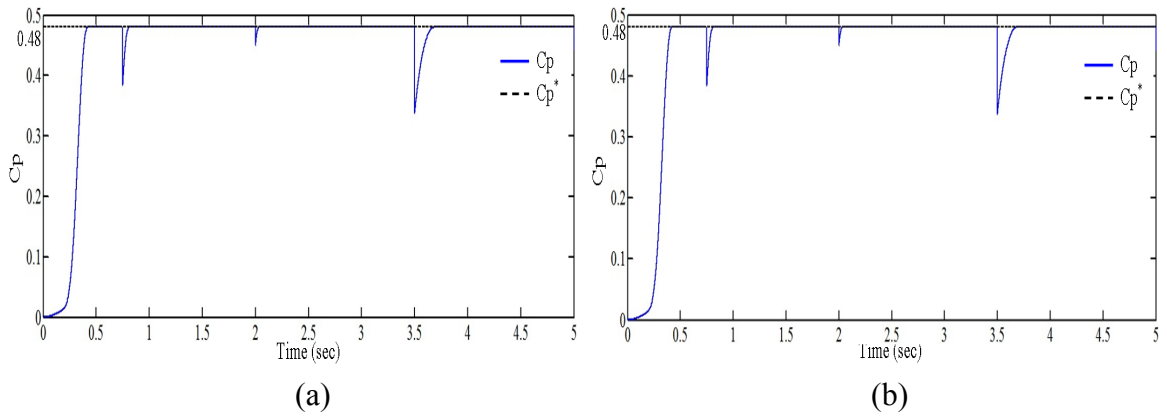
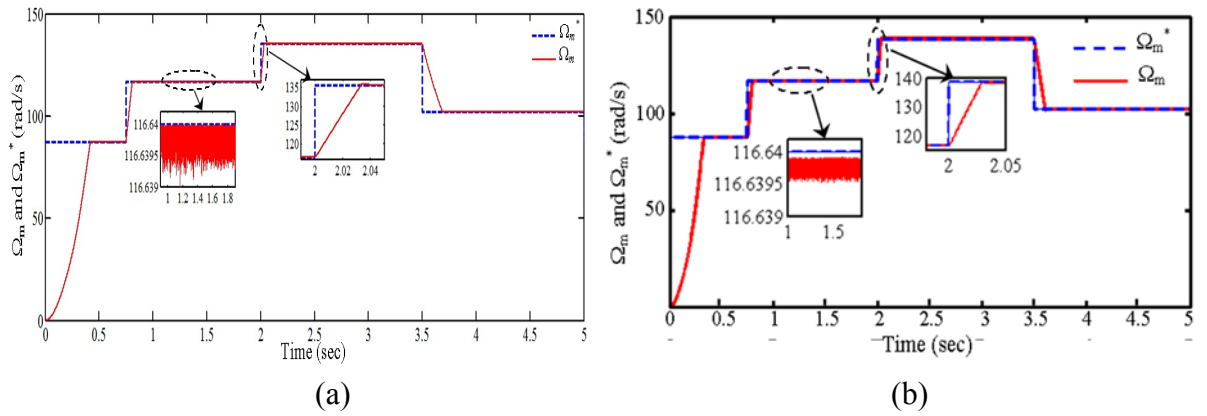
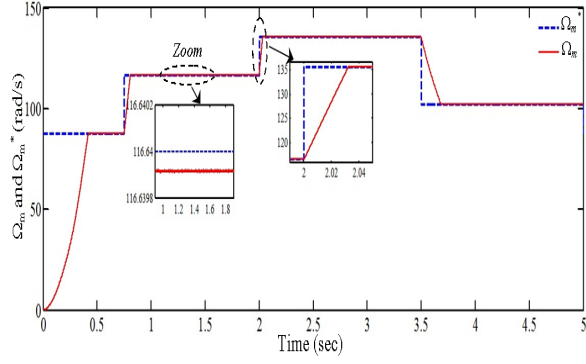


Fig. 11 Power coefficient (a) conventional SMC, (b) proposed SMC.





(c)

Fig. 12 Generator speed. (a) Conventional SMC, (b) proposed SMC without the switching gains adaptation, (c) proposed SMC.

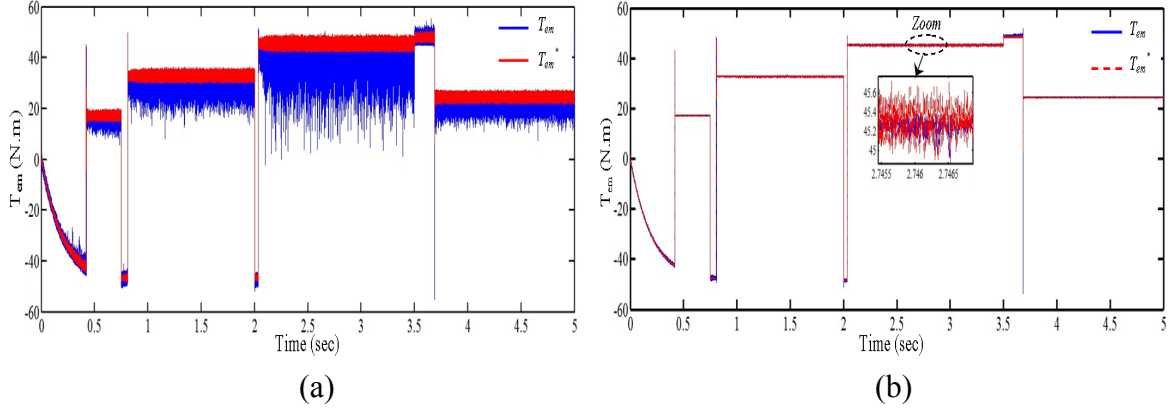


Fig. 13 Electromagnetic torque of the WFSG (a) conventional SMC, (b) proposed SMC.

Figs. 14(a) and 14(c) show the stator  $q$ -axis current components which control the electromagnetic torques. Both responses exhibit a peak during each step change in the wind speed that is more important in the case of the conventional SMC.

Usually, chattering is more important in the stator  $q$ -axis current reference in conventional SMC due to the discontinuous function and switching gain. In the proposed SMC, chattering is significantly reduced with the use of a continuous function.

The stator currents waveforms of the WFSG for both controllers are presented in Figs. 15(a) and 15(b). These figures show a proportional increase in the stator currents with the wind speed as expected. The stator phase current has a lower THD (10.43%) in the case of the proposed SMC as compared to the conventional SMC (14.84%).

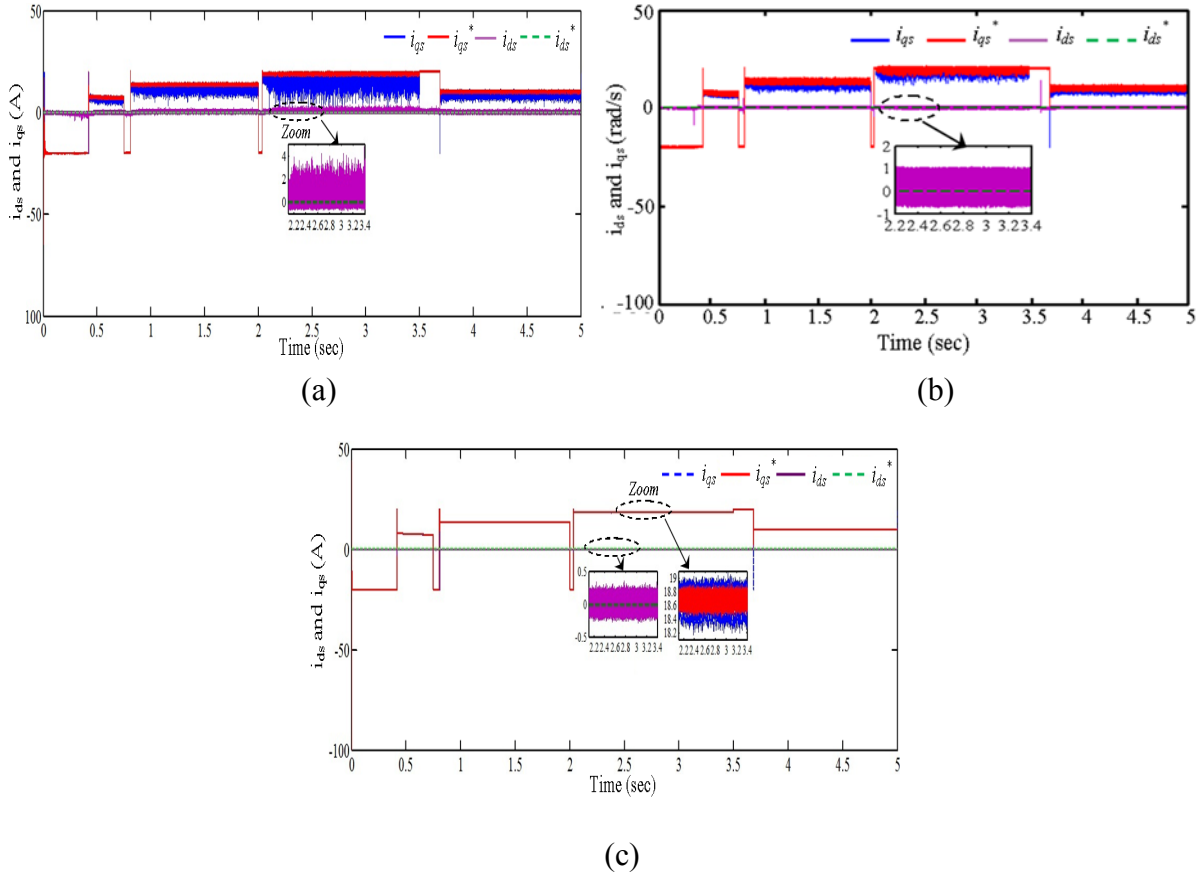


Fig. 14 Direct and quadratic stator current (a) conventional SMC, (b) proposed SMC without the switching gains adaptation, (c) proposed SMC.

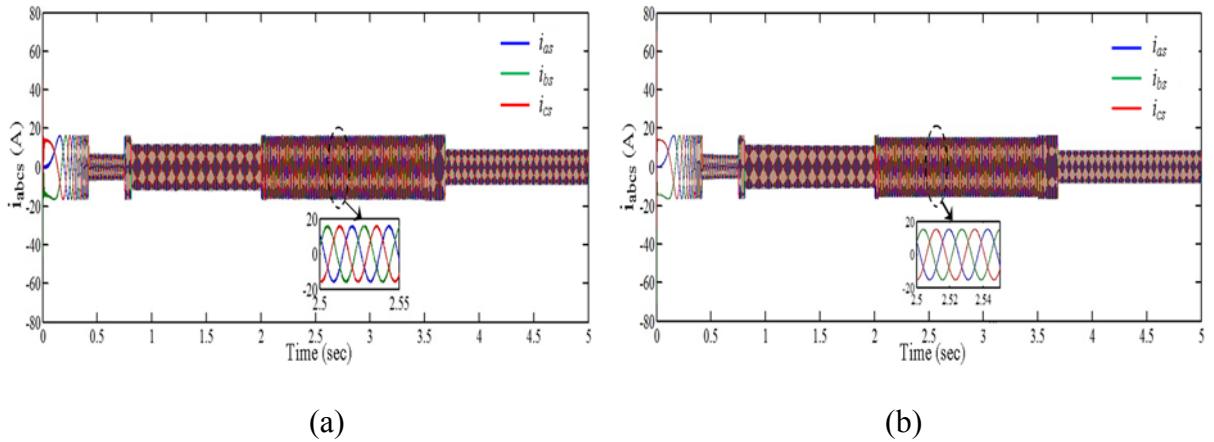


Fig. 15 Stator current of the WFSG (a) conventional SMC, (b) proposed SMC.

To verify the effect of the proposed switching gain adaptation simulation results for the rotor speed and stator current without the switching gains adaptation are presented, respectively in Fig. 12(b) and Fig. 14(b). This can be clearly seen by comparing Fig. 12(a), Fig. 12(b) and Fig. 12(c) or Fig. 14(a), Fig. 14(b) and Fig. 14(c). These results demonstrate that the gain adaptation method used in the proposed control approach is able to efficiently attenuate the chattering.

To further demonstrate the effectiveness of the proposed control, a simulation result is presented to compare the proposed control strategy with a standard proportional-integral (PI) controller and a fuzzy logic controller (FLC) respectively. Fig. 16 shows the rotor speed, quadrature stator current and direct stator current with these three control methods. These results show that the proposed control strategy has a better response characteristics in terms of settling time and overshoot as compared to both PI control and the FLC. Furthermore, the oscillations in the system states have been considerably reduced.

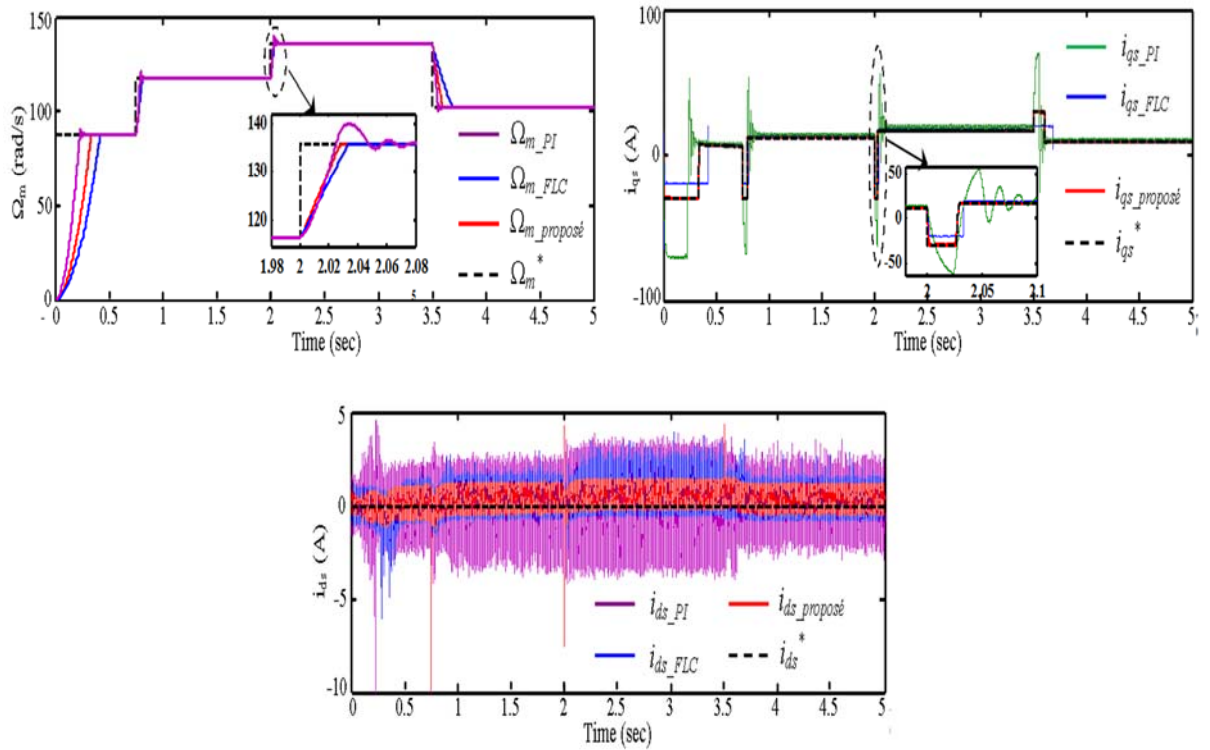


Fig. 16 System performance under step-change wind for three controllers (PI controller, FL controller and proposed controller).

## B. Random Wind

For this simulation scenario both converters (MSC and GSC) are considered. In this simulation, the response of the three controllers is tested and compared under random variation of the wind speed (Fig. 17).

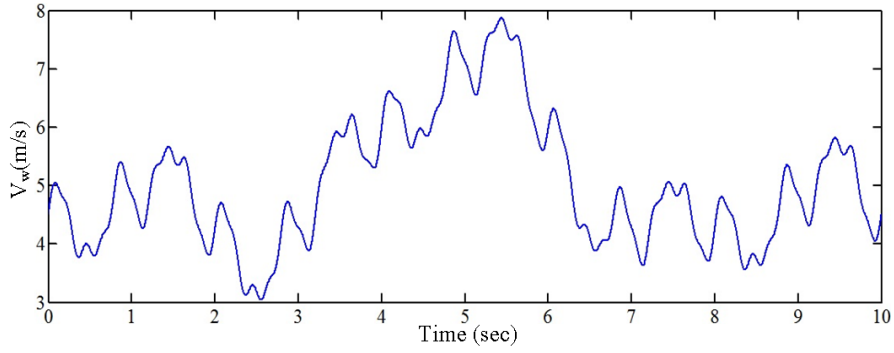
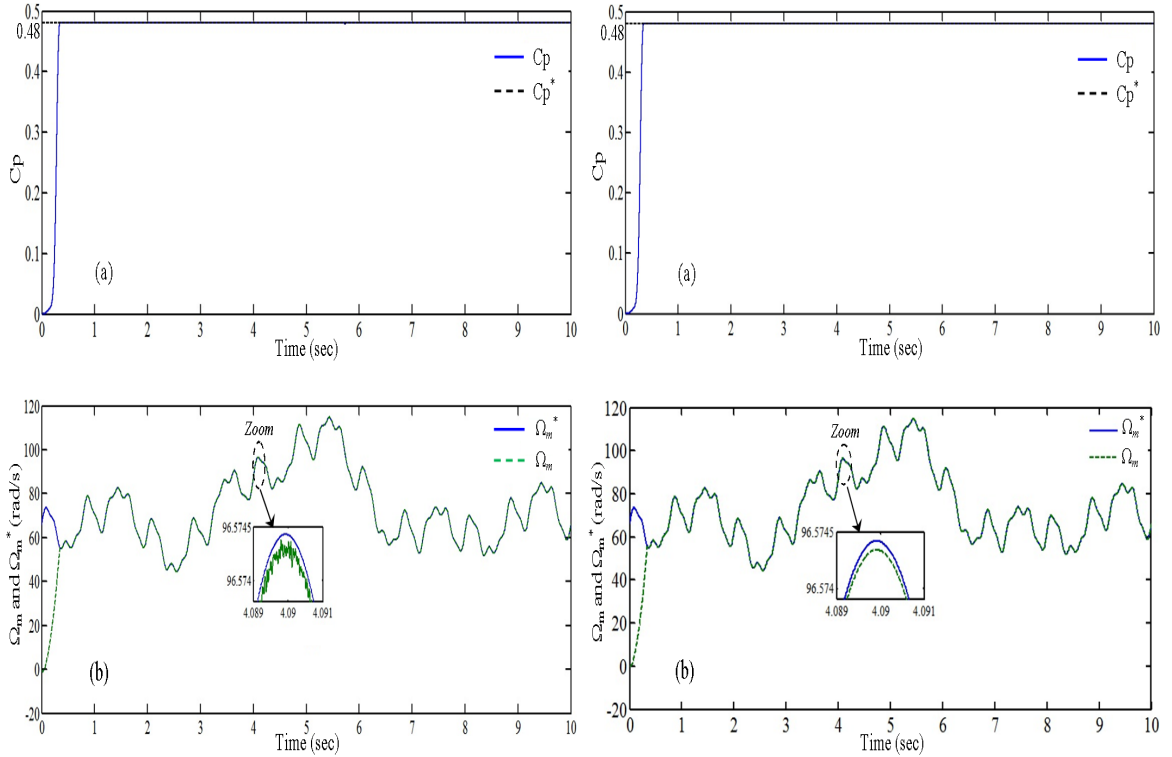


Fig. 17 Random wind speed profile.

The simulation results for the MSC when using the conventional SMC, the proposed SMC, and FLC are illustrated in Fig. 18(A), 18(B) and Fig. 19, respectively. It can be seen that all three controllers lead to a good steady-state performance. The proposed SMC, and FLC have a faster transient response and smoother operation as compared to the conventional SMC as shown in Fig. 18(B) and Fig. 19. The FLC has a fast transient response and good tracking of the reference, however, as shown in Fig. 19, the stator current waveforms presents some large ripples at 5 sec and 6 sec.

The results related to GSC with both controllers are presented in Figs. 20(A) and 20(B) respectively. These results demonstrate a significant reduction in the chattering with the proposed SMC as compared to the conventional SMC.



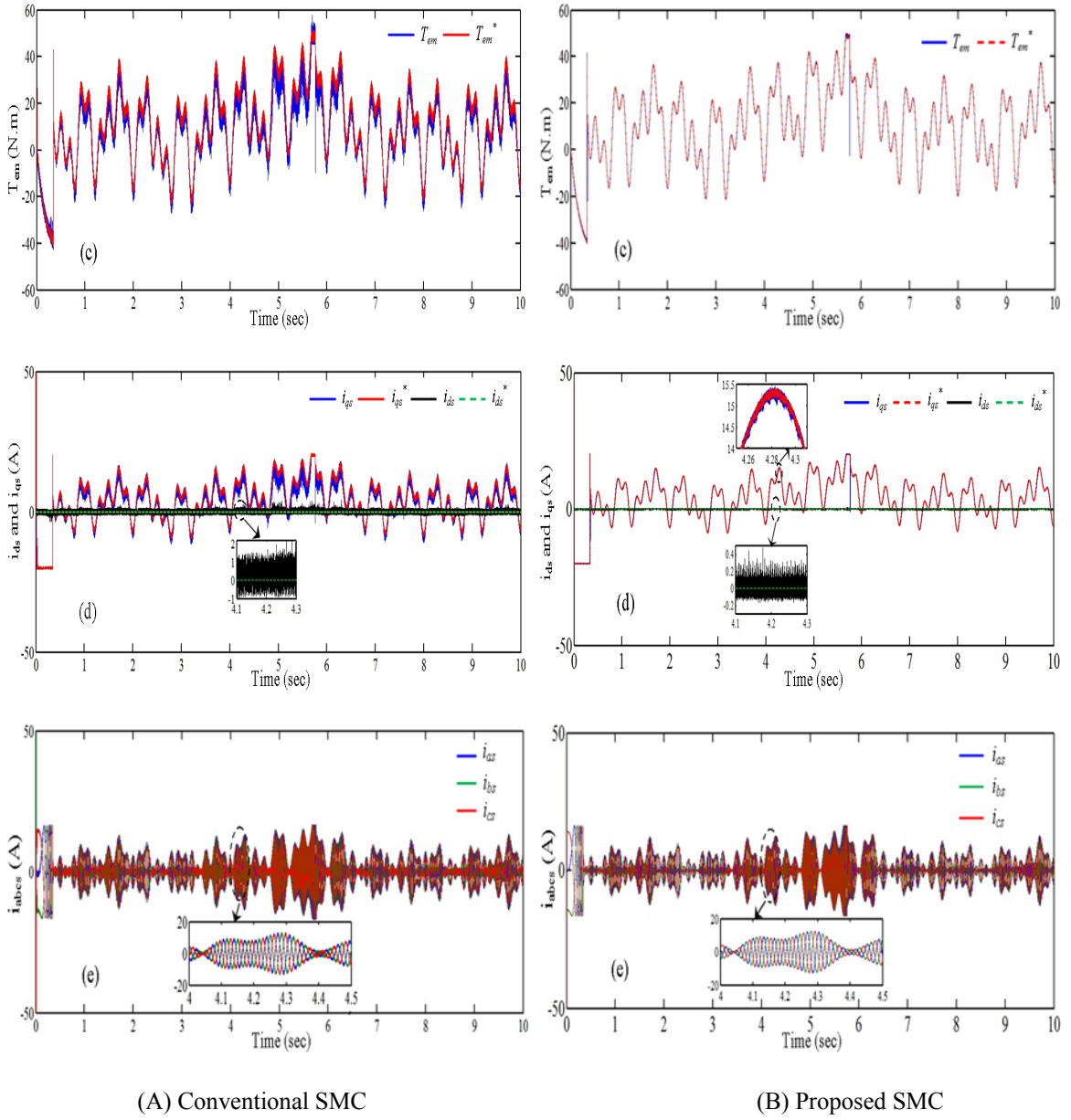
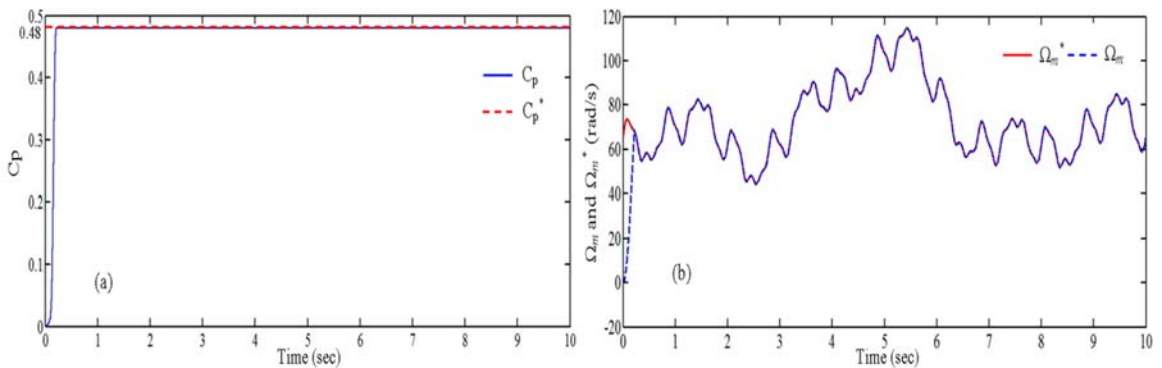


Fig. 18 Performance of the MSC for both controllers. (a) Power coefficient, (b) Generator speed, (c) Electromagnetic torque of the WFSG, (d) Direct and quadratic stator current, (e) Stator current of the WFSG.



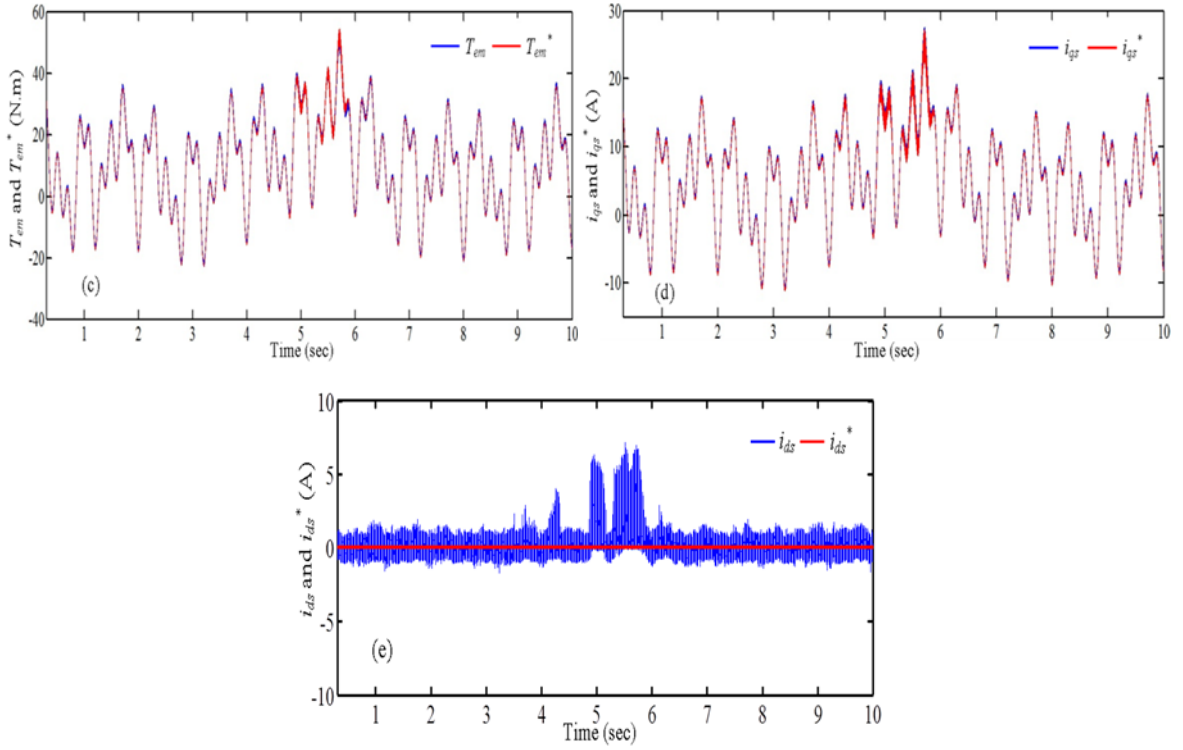
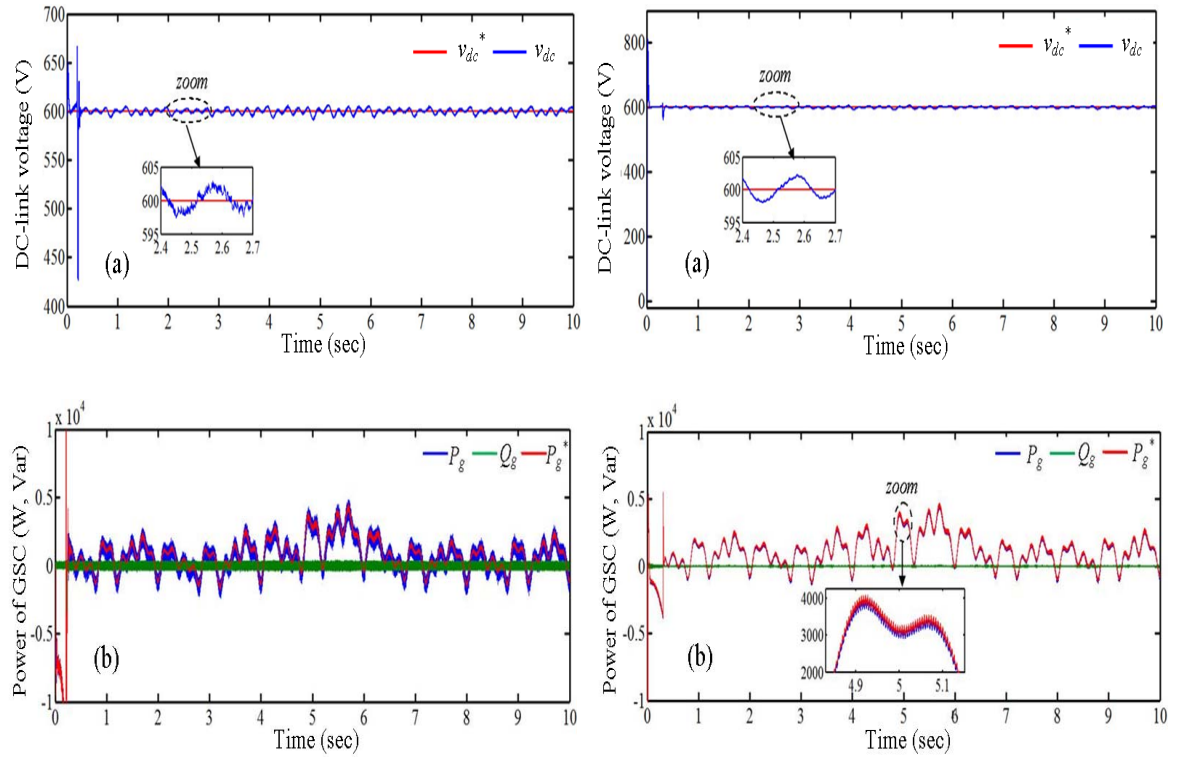


Fig. 19 Performance of the MSC for fuzzy logic control. (a) Power coefficient, (b) Generator speed, (c) Electromagnetic torque of the WFSG, (d) Quadratic stator current, (e) Direct stator current of the WFSG.



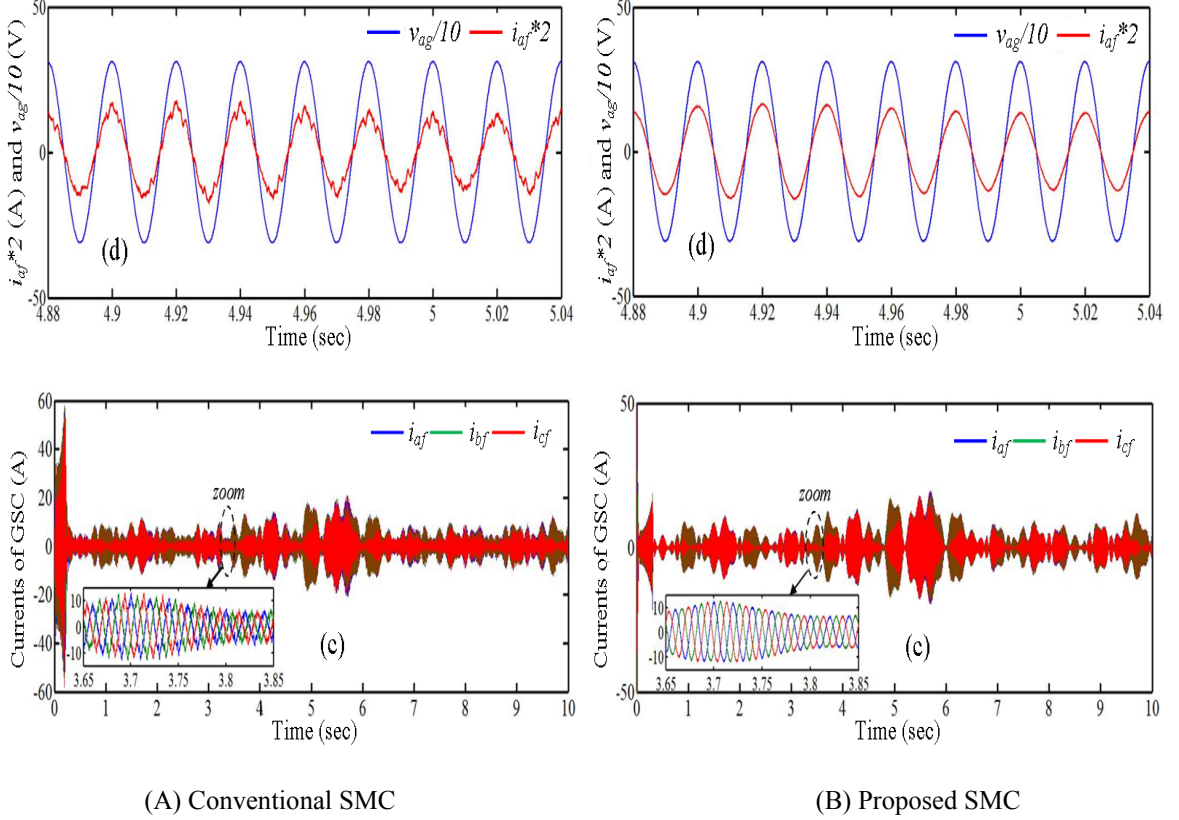


Fig. 20 Performance of the GSC for both controllers. (a) DC-link voltage, (b) Power of GSC, (c) Currents of GSC, (d) Zoom of grid current and voltage of phase a.

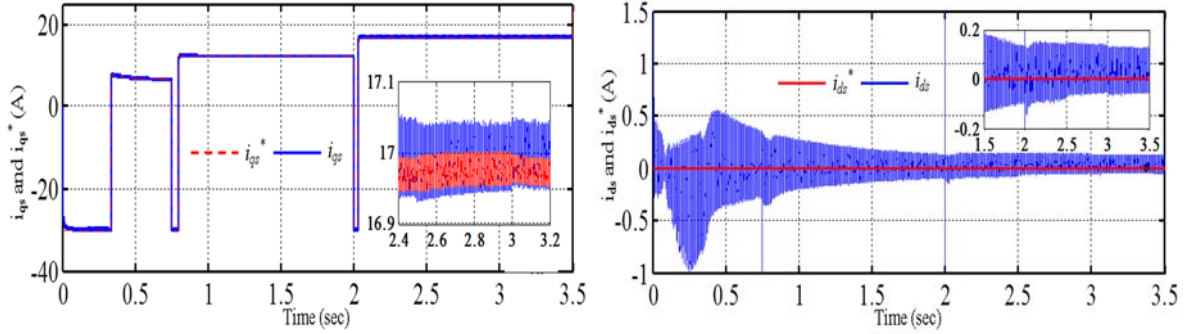
### C. Robustness

The aim of this test is to analyze the influence of the WFSG's parameters variations on the performance of the controllers. The following two tests are performed without changing the parameters of the controllers obtained previously:

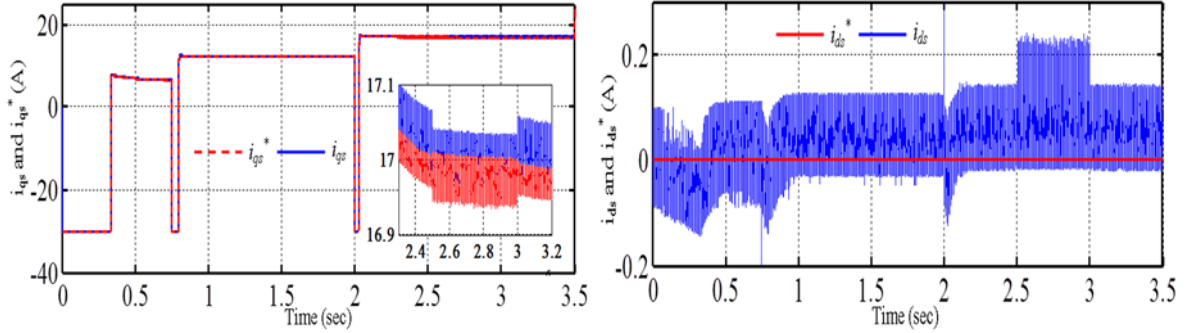
- The value of the stator inductance  $L_q$  is increased by 50% from its nominal value.
- The value of the mutual inductance  $M_{sf}$  is decreased by 10% from its nominal value.

The effect of these parameter variations on the response of the  $d$ - and  $q$ -axis components of the stator current for both controllers is shown in Figs. (21) and (22).

These results demonstrate that the proposed SMC controller is more robust and less sensitive to machine parameter variations as compared to the conventional SMC.

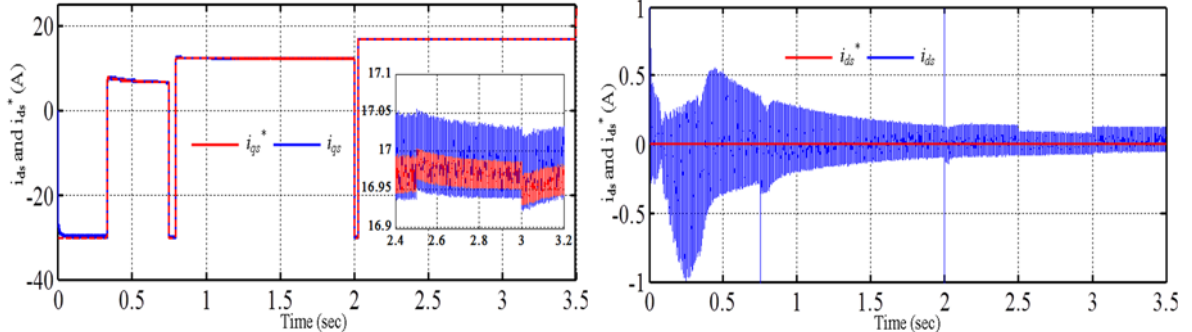


(a) Results with the proposed SMC.

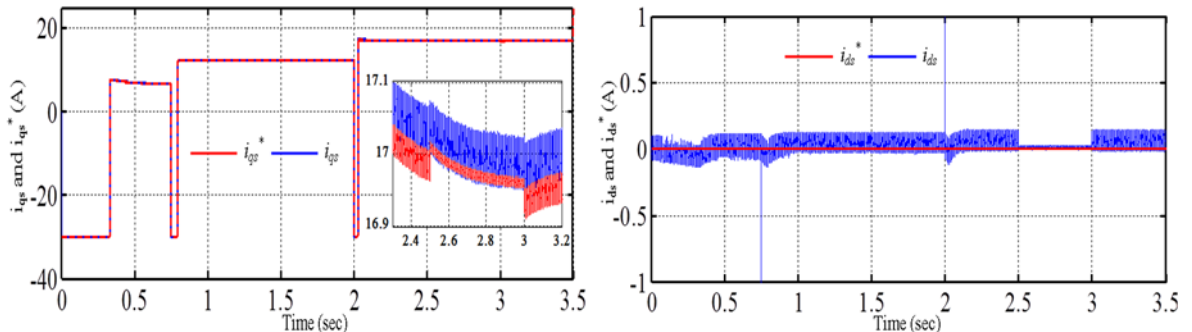


(b) Results with the conventional SMC.

Fig. 21 Effect of machine's parameters variation (+50% of  $L_q$ ) .



(a) Results with the proposed SMC.



(b) Results with the conventional SMC.

Fig. 22 Effect of machine's parameters variation (-10% of  $M_{sf}$ ).

## X. CONCLUSION

In this paper, the modeling and control strategy of a wound-field synchronous generator (WFSG) variable speed wind energy conversion systems (WECS) is presented. The variability and intermittent nature of wind speed and the inherent nonlinear characteristics and uncertainties characterizing the dynamics of the WECS system makes the design of a controller for the system challenging. The paper proposes a new sliding-mode control derived from the sliding surface. Furthermore, the proposed control strategy is designed to maximize the power captured by the wind turbine. The main contribution consists in showing that the problem of chattering which is inherent in conventional SMC has been significantly reduced by replacing the discontinuous function of conventional SMC with a fast sigmoid function with varying boundary layer and adjustable the switching gain using a simple set of fuzzy logic rules. The proposed SMC was compared with the conventional SMC under different simulation scenarios and the results demonstrate an improvement in the robustness and reference tracking accuracy of the proposed SMC in addition to its ability to reduce chattering.

## XI. LIST OF SYMBOLS AND ABBREVIATIONS

### A. Abbreviations

- DFIG** doubly fed induction generator
- FOC** field-oriented control
- FLC** fuzzy logic control
- GSC** grid side converter
- LQG** linear-quadratic-gaussian controller
- GSC** grid side converter
- MPPT** maximum power point tracking
- MSC** machine side converter
- PID** proportional–integral
- PID** proportional–integral–derivative
- PMSG** permanent magnet synchronous generator
- PWM-VSC** pulse width modulation voltage source converter
- RST** R-S-T are polynomials
- SCIG** squirrel-cage induction generator
- SMC** sliding mode control

**TSR** tip speed ratio

**WECS** wind energy conversion on system

**WFSG** wound field synchronous generator

## B. Symbols

$v_s, i_s$	stator voltages and currents	$M_{SD}$	mutual inductance between the stator and direct damper
$v_f, i_f$	voltage and current of the main field winding	$M_{SQ}$	mutual inductance between the stator and quadrature damper
$i_D, i_Q$	direct and quadrature damper currents	$\omega_e, \omega_g$	electrical and grid angular frequencies
$r_s, r_f, r_D, r_Q$	Resistances of the stator, main field and dampers	$\theta_g$	grid voltage angle
$L_d, L_q$	inductances of the direct and quadrature stator windings	$i_g, v_g$	grid-side converter (GSC) output voltage and current
$L_f, L_D, L_Q$	inductances of the main field, direct and quadrature dampers	$P_s, Q_s$	stator active and reactive powers
$M_{sf}$	mutual inductance between direct stator winding and main field	$P_g, Q_g$	GSC output active and reactive powers
$M_{fD}$	mutual inductance between main field winding and direct damper		

## REFERENCES

- [1] D. Petković, Ž. Ćojašić, and V. Nikolić, “Adaptive neuro-fuzzy approach for wind turbine power coefficient estimation,” *Renewable and Sustainable Energy Reviews*, vol. 28, pp. 191–195, 2013.
- [2] W.-M. Lin, C.-M. Hong, T.-C. Ou, and T.-M. Chiu, “Hybrid intelligent control of pmsg wind generation system using pitch angle control with rbf,” *Energy Conversion and Management*, vol. 52, no. 2, pp. 1244–1251, 2011.
- [3] F. Blaabjerg, F. Iov, Z. Chen, and K. Ma, “Power electronics and controls for wind turbine systems,” in *Energy Conference and Exhibition (EnergyCon), 2010 IEEE International*, pp. 333–344, IEEE, 2010.
- [4] S. Shukla and P. Maurya, “Generator and power converter topology for wind energy conversion system,” 2012.
- [5] M. E. TOPAL and L. T. ERGENE, “Designing a wind turbine with permanent magnet synchronous machine,” *IJU-Journal of Electrical & Electronics Engineering*, vol. 11, no. 1, pp. 1311–1317, 2011.
- [6] V. Calderaro, V. Galdi, A. Piccolo, and P. Siano, “A fuzzy controller for maximum energy extraction from variable speed wind power generation systems,” *Electric Power Systems Research*, vol. 78, no. 6, pp. 1109–1118, 2008.
- [7] V. Galdi, A. Piccolo, and P. Siano, “Exploiting maximum energy from variable speed wind power generation systems by using an adaptive takagi–sugeno–kang fuzzy model,” *Energy Conversion and Management*, vol. 50, no. 2, pp. 413–421, 2009.
- [8] F. Poitiers, T. Bouaouiche, and M. Machmoum, “Advanced control of a doubly-fed induction generator for wind energy conversion,” *Electric Power Systems Research*, vol. 79, no. 7, pp. 1085–1096, 2009.

- [9] K. Tahir, C. Belfedal, T. Allaoui, and M. Doumi, “Proposal of a new hybrid control strategy for dynamic performance improvement of wound field synchronous generator-based wind turbines,” *J. Renewable Sustainable Energy* 7, 043113 (2015).
- [10] A. Kerboua, “Hybrid fuzzy sliding mode control of a doubly-fed induction generator speed in wind turbines,” *Journal of Power Technologies*, vol. 95, no. 2, p. 126, 2015.
- [11] F. Amrane, A. Chaiba, and S. Mekhilef, “High performances of grid-connected DFIG based on direct power control with fixed switching frequency via MPPT strategy using MRAC and neuro-fuzzy control,” *Journal of Power Technologies*, vol. 96, no. 1, p. 27, 2016.
- [12] A. G. Aissaoui, M. Abid, and A. Tahour, “Application of fuzzy sliding mode technique in controller and observer of synchronous motor,” in *Energy Conference and Exhibition (EnergyCon), 2010 IEEE International*, pp. 440–445, IEEE, 2010.
- [13] S. Chi, Z. Zhang, and L. Xu, “Sliding-mode sensorless control of direct-drive pm synchronous motors for washing machine applications,” *IEEE Transactions on Industry Applications*, vol. 45, no. 2, pp. 582–590, 2009.
- [14] H. Amimeur, D. Aouzelag, R. Abdessemed, and K. Ghedamsi, “Sliding mode control of a dual stator induction generator for wind energy conversion systems,” *International Journal of Electrical Power & Energy Systems*, vol. 42, no. 1, pp. 60–70, 2012.
- [15] O. Barambones, J. A. Cortajarena, P. Alkorta, and J. M. G. de Durana, “A real-time sliding mode control for a wind energy system based on a doubly fed induction generator,” *Energies*, vol. 7, no. 10, pp. 6412–6433, 2014.
- [16] K. Boulaam and A. Boukhelifa, “A fuzzy sliding mode control for dfig-based wind turbine power maximisation,” 2014.
- [17] S. Rajendran and D. Jena, “Variable speed wind turbine for maximum power capture using adaptive fuzzy integral sliding mode control,” *Journal of Modern Power Systems and Clean Energy*, vol. 2, no. 2, pp. 114–125, 2014.
- [18] Patnaik RK, Dash PK, Mahapatra K. Adaptive terminal sliding mode power control of DFIG based wind energy conversion system for stability enhancement. *Int. Trans. Electr. Energ. Syst.* 2016; 26:750–782.
- [19] A. D. Wright, “Wind turbine control systems,” in *Wind Turbine Technology : Fundamental Concepts in Wind Turbine Engineering, Second Edition*, ASME Press, 2009.
- [20] Tripathi SM, Tiwari AN, Singh D. Optimum design of proportional-integral controllers in grid integrated PMSG-based wind energy conversion system. *Int. Trans. Electr. Energ. Syst.* 2016; 26:1006–1031.
- [21] W. Qiao, L. Qu, and R. G. Harley, “Control of IPM synchronous generator for maximum wind power generation considering magnetic saturation,” *IEEE Transactions on industry applications*, vol. 45, no. 3, pp. 1095–1105, 2009.
- [22] A. Barakat, S. Tnani, G. Champenois, and E. Mouni, “Analysis of synchronous machine modeling for simulation and industrial applications,” *Simulation Modelling Practice and Theory*, vol. 18, no. 9, pp. 1382–1396, 2010.
- [23] O. Anaya-Lara, N. Jenkins, J. Ekanayake, P. Cartwright, and M. Hughes, *Wind energy generation : modelling and control*. John Wiley & Sons, 2011.
- [24] J. Yan, H. Lin, Y. Feng, and Z. Zhu, “Control of a grid-connected direct-drive wind energy conversion system,” *Renewable Energy*, vol. 66, pp. 371–380, 2014.
- [25] J.-J. E. Slotine, W. Li, et al., *Applied nonlinear control*, vol. 199. prentice-Hall Englewood Cliffs, NJ, 1991.
- [26] J.-C. Lo and Y.-H. Kuo, “Decoupled fuzzy sliding-mode control,” *IEEE Transactions on Fuzzy systems*, vol. 6, no. 3, pp. 426–435, 1998.
- [27] A. Mohamed, A. ghani AISSAOUI, and H. BOOUNOUA, “Sliding mode application in speed and flux control of an induction machine,” *IU-Journal of Electrical & Electronics Engineering*, vol. 6, no. 2, pp. 197–204, 2006.
- [28] H. Lee and V. I. Utkin, “Chattering suppression methods in sliding mode control systems,” *Annual reviews in control*, vol. 31, no. 2, pp. 179–188, 2007.
- [29] Y. Errami, M. Ouassaid, and M. Maaroufi, “A performance comparison of a nonlinear and a linear control for grid connected PMSG wind energy conversion system,” *International Journal of Electrical Power & Energy Systems*, vol. 68, pp. 180–194, 2015.

[30] M. Abdelrahem, C. Hackl, and R. Kennel, “Model predictive control of permanent magnet synchronous generators in variable-speed wind turbine systems,” *Proceedings of Power and Energy Student Summit (PESS 2016)*, 2016.

[31] M. H. Mobarak, M. Abdelrahem, N. Stati, and R. Kennel, “Model predictive control for low voltage ride-through capability improvement of variable-speed wind energy conversion systems,” in *Industrial Electronics (INDEL), International Symposium on*, pp. 1–6, IEEE, 2016.

## APPENDICES

### Appendix A: Specification of wind turbine

The following generic equation is used for  $C_p(\lambda, \beta)$  based on the turbine characteristics:

$$C_p(\lambda, \beta) = c_1 \left( \frac{C_2}{\lambda_i} - c_3 - 3\beta - c_4 \right) \exp \left( -\frac{c_5}{\lambda_i} \right) + c_6 \lambda \quad (A1)$$

With

$$\frac{1}{\lambda_i} = \frac{1}{\lambda + 0.08\beta} - \frac{0.035}{\beta^3 + 1} \quad (A2)$$

And  $c_1 = 0.5176$ ,  $c_2 = 116$ ,  $c_3 = 0.4$ ,  $c_4 = 5$ ,  $c_5 = 21$  and  $c_6 = 0.0068$ .

### Appendix B: Parameters used in the simulation models

Parameters	Symbol	Value
<b>Turbine</b>		
Rated power of the turbine	$P_t$	10 (kW)
Density area	$\rho$	1.225 ( $\text{kg.m}^{-2}$ )
Radius of the turbine	$R$	3 (m)
Number of blades		3
Gear ratio	$G$	5.4
Viscous friction coefficient	$f$	0.017 ( $\text{N.m.s}^{-1}$ )
<b>WFSG</b>		
Rated power of the generator	$S_n$	7.5 (kVA)
Stator resistance	$r_s$	1.19 ( $\Omega$ )
Rotor resistance	$r_f$	3.01 ( $\Omega$ )
Phase to phase rated voltage	$U_{rms}$	400 (V)
Direct synchronous reactance	$X_d$	1.4 (p.u)
Transverse synchronous reactance	$X_q$	0.7 (p.u)
Open circuit transient time constant	$T_{d0}''$	522 (ms)
Direct transient synchronous reactance	$X_d'$	0.099 (p.u)
Direct sub-transient synchronous reactance	$X_d''$	0.049 (p.u)
Direct transient time constant	$T_d'$	40 (p.u)
Direct sub-transient time constant	$T_d''$	3.7 (ms)
Armature time constant	$T_a$	6 (ms)
<b>Grid</b>		
DC-Link voltage	$v_{dc}$	600 (V)
DC capacitance	$C$	1500 ( $\mu\text{F}$ )
Effective voltage	$V_{rms}$	220 (V)
Frequency	$f_s$	50 (Hz)
Leakage resistance	$R_f$	1 ( $\Omega$ )
The leakage inductance	$L_f$	12 (mH)